# Title: Employing Metadynamics to Predict the Membrane Partitioning of Carboxy-2*H*-Azirine Natural Products

## Authors:

Clyde A. Daly Jr.*[,1] (ORCID 0000-0003-2051-0561), Leah M. Seebald[1] (ORCID 0000-0001-8890-8985) and Emma Wolk[1]

[1] Haverford College
Department of Chemistry
370 Lancaster Ave
Haverford, PA 19041
United States of America

*Corresponding author, 610-896-1000, cdaly2@haverford.edu

# Abstract

Natural products have diverse chemical structures and biological activities which often serve as sources of new therapeutic agents. Those containing a carboxy-2*H*-azirine moiety are an exciting target for investigation due in part to the broad-spectrum antimicrobial activity these compounds have and the significant chemical space for novel therapeutic development offered by this unique scaffold. The carboxy-2*H*-azirine moiety, including those appended to well-characterized chemical scaffolds, is understudied, which creates a challenge for understanding potential modes of inhibition. In particular, some known natural product carboxy-2*H*-azirines have long hydrophobic tails, which might lead to amphipathicity and implicate them in membrane associated processes. Metadynamics is an effective method for calculating the free energy changes associated with membrane embedding processes. In this study, we examined a small set of carboxy-2*H*-azirine natural products, including analogs with long alkyl chains, geometric isomers, and one comprising the simple carboxy-2*H*-azirine core. We compared the physiochemical properties of these compounds to those of established membrane embedders with similar chemical scaffolds. This was intended to isolate the physiochemical properties of the carboxy-2*H*-azirine group and understand molecular influences of this moiety on membrane partitioning. To accomplish this, we developed a force field for the 2*H*-azirine functional group and performed metadynamics simulations of the partitioning into a model membrane (75 % POPE, 25 % POPG) from aqueous solution. We determine that the carboxy-2*H*-azirine functional group is likely hydrophilic, imbuing the long chain analogs with amphipathicity similar to the known membrane binding molecules to which they were compared. For the long chain analogs, the carboxy-2*H*-azirine headgroup stays within 1 nm of the phosphate layer, while the carboxy-2*H*-azirines lacking the long alkyl chain partitions completely into aqueous solution.

# Introduction

The alarming global increase in antimicrobial resistance has created a pressing need to expand the chemical space of antimicrobials to mitigate infectious diseases.[1] Natural products containing a carboxy-2*H*-azirine moiety have garnered attention for demonstrating moderate antibacterial and antifungal inhibition against resistant microbes.[2–4] Thus far, nine such carboxy-2*H*-azirine natural products have been identified; the structures are shown in **Figure 1**. These unique products have been isolated from marine sponge sources (*Dysidea fragilis* **1**-**4**, and *Siliquaria spongia,* **3**-E-An-Me)[4–6] and from bacterial sources (marine cyanobacterium *Caldora sp*., **5**-E-Dy-H and *Streptomyces aureus,* **6**-Az-H).[7,8] These products (**1**-**6**) display a high degree of chemical similarity; many have a long alkyl chain and are geometric isomers or contain terminal halogenated chains. Notably, **1**-**4** are have a methyl ester and **5**-E-Dy-H and **6**-Az-H were characterized as a free acid. Compound **6**-Az-H is the smallest of these natural products, composed of the minimal structural core, the carboxy-2*H*-azirine, but lacking the long alkyl chain.

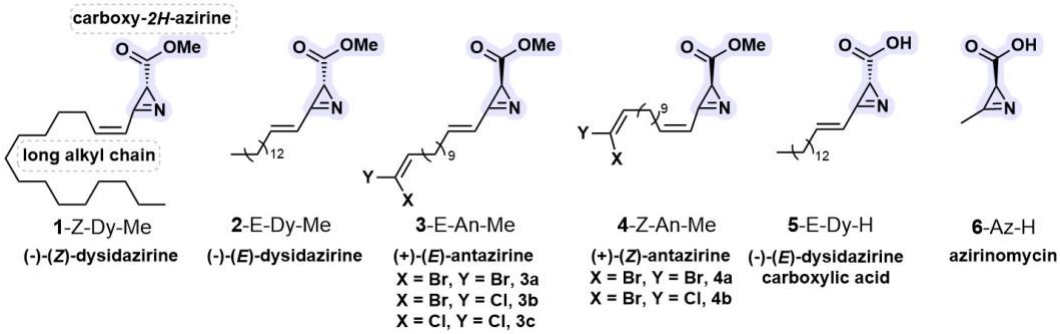


***Figure 1:*** *Structures of the nine known natural products that contain a carboxy-2H-azirine. The characteristic carboxy-2H-azirine moiety is highlighted in purple.*

Structural features of natural products can often supply hints to infer biological targets. For example, many natural products known to inhibit membrane protein activity or disrupt membrane integrated processes have a distinctive amphipathic scaffold.[9] Identifiable polar groups can include carbohydrates, nucleosides, peptides, and can also include simple polar functional groups such as carboxylic acids and phosphates. Key non-polar features include both long saturated and unsaturated hydrocarbons or more complex hydrophobic scaffolds like steroids[10] or terpenes.[11] Two examples of distinctly amphipathic natural products with known mechanisms of antimicrobial inhibition are shown in **Figure 2**. These examples include tunicamycin (**Figure 2A**), a potent natural product inhibitor that targets bacterial cell wall biosynthesis by targeting a polytopic phosphoglycosyl transferase (polyPGT), an integral membrane protein, ultimately inhibiting *N*-linked glycosylation.[12] Structurally, tunicamycin comprises a long alkyl chain decorated with carbohydrates and a uridine nucleoside. It its action as an inhibitor, the long alkyl chain of tunicamycin embeds in the lipid bilayer, allowing it to out compete the lipid substrate in the polyPGT hydrophobic binding pocket.[12] The carbohydrates and nucleoside both mimic the native soluble substrate that polyPGTs acts on, serving as a bi-substrate transition state analog.[13] Another example includes echinocandin B (**Figure 2B**), a lipopeptide antifungal that contains a linoleic acid side chain and a hexacyclic peptide core. It non-competitively inhibits the synthesis of β-D-glucan in fungal cell walls. During this process, the long hydrophobic alkyl chain embeds

in the fungal cell membrane and the cyclic lipopeptide core imbues water solubility.[14] Synthetic derivatives have been developed to tune antifungal activity and physiochemical properties to improve efficacy.[15]

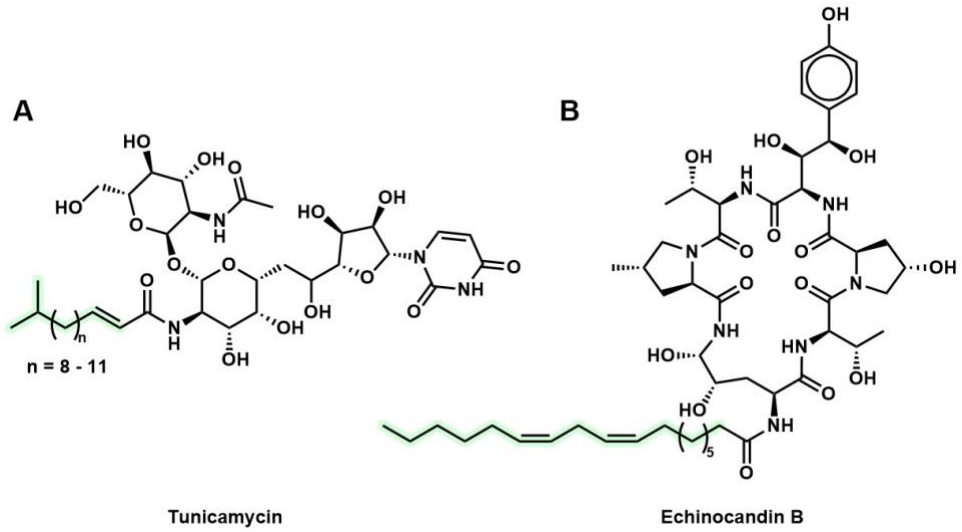


***Figure 2:*** *Two examples of potent natural product antimicrobials with amphipathic structures. The hydrophobic alkyl chain is highlighted in green.* ***A*** *Tunicamycin is an antibiotic that inhibits bacterial cell wall biosynthesis by inhibiting N-linked glycosylation.* ***B*** *Echinocandin B is an antifungal that inhibits the synthesis of β-D-glucan in fungal cell walls.*

This correlation between amphipathic structure and inhibition of a membrane target may be hypothesized to exist for the carboxy-2*H*-azirine natural products. Compounds **1** – **5** all bear a long hydrophobic alkyl chain ranging from 16 to 18 carbons, suggestive of integration into a membrane lipid bilayer. On the other hand, the physiochemical properties of carboxy-2*H*-azirines are not nearly as well-established as typical moieties found in natural products. The 2*H*-azirine is the smallest unsaturated nitrogen heterocycle. This strained ring can be thermally unstable and is often used as a synthetic intermediate to access azole and azine derivatives in addition to complex polyheterocyclic scaffolds.[16] Substituted 2*H*-azirines can achieve uniquely balanced stability and reactivity, such that some of these molecules can be utilized in biological environments. For example, phenyl 2*H*-azirines and internal 2*H*-azirines have been employed as chemoselective activity probes in live cells,[17] and the phenyl 2*H*-azirine probes have been employed to target enzymes from membrane protein isolates.[18] The biosynthesis and isolation of these natural products with 2*H*-azirines suggests the carboxy group can enhance stability, with the exception of **6**-Az-H, which was found to degrade upon isolation by solvent removal.[6] These examples all highlight the unique chemical space that 2*H*-azirine containing compounds occupy, yet the key determinants for these varied physiochemical properties are not yet well understood. This uncertainty poses a unique challenge for predicting the mode of inhibition of 2*H*-azirine containing natural products. While the long alkyl chains of compounds **1**-**5** are suggestive of lipid embedding, the influence of the carboxy-2*H*-azirine on these membrane interactions is unclear.

Without such tools, we first look to structurally similar molecules to help guide predictions of the physicochemical properties of a carboxy-2*H*-azirine interacting with a membrane lipid bilayer. Compounds **1**-**5** share a striking structural resemblance with sphingosine (**Figure 3**).[19]

Sphingosine is an membrane-embedded, amphipathic biological molecule which is a member of the sphingolipid family. This family of molecules plays important roles in cell wall integrity, cell recognition and signaling, and can be further elaborated to perform a myriad of essential biological functions.[20,21] Sphingosine, elaborated analogs of sphingosine such as sphingosine-1-phosphate, as well as compounds **1**-*Z*-Dy-Me, **2**-*E*-Dy-Me and **5**-*E*-Dy-H, all share a linear carbon chain comprising 18 carbons. Compounds **1**-**5**, sphingosine, and analogs are unsaturated between C4 and C5, with **1**-*Z*-Dy-Me and **4**-Z-An-Me with Z configuration. The structural similarity of sphingolipids with many of the carboxy-2*H*-azirine natural products strongly supports analogous amphipathicity for products **1**-**5**. Thus, similar membrane orientation would be expected, wherein the hydrophobic chains of **1**-**5** would bury in the membrane lipid bilayer, and orient the carboxy-*2H*-azirine towards the hydrophilic heads of the polar lipid headgroups of the membrane. The greatest uncertainty in this prediction arises from the difference in oxidation at C1 of **1**-**5** and the understudied properties of the 2*H*-azirine heterocycle, especially related to hydrophilicity.

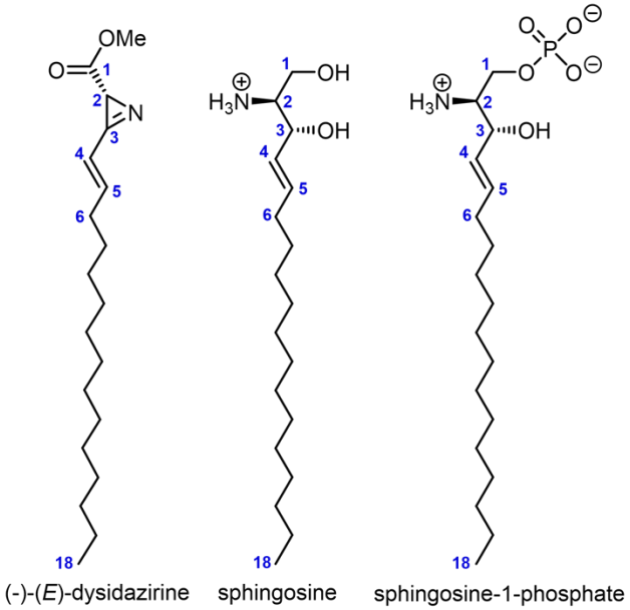


(-)-(*E*)-dysidazirine sphingosine sphingosine-1-phosphate

***Figure 3:*** *Structure of **2**-E-Dy-Me, a representative carboxy-2H-azirine natural product, compared to the structures of sphingosine and sphingosine-1-phosphate. Carbons are numbered in blue according to IUPAC rules. Notable similarities include the alkyl chain length, the C4-C5 unsaturation, and the nitrogen and oxygen heteroatoms at C1 and C2.*

Computational tools such as molecular dynamics (MD) have been used to make predictions of membrane partitioning, permeability, and small molecule embedding.[22–26] In MD simulations, atoms are treated as classical particles and are simulated using numerical integration of Newton's laws of motion.[27] The potential energy surface, called a "force field," used in these simulations is obtained from quantum chemistry calculations and/or experimental observations.[28] While extensive force fields for biomolecules and many small molecules exist, there has been little effort to parameterize carboxy-2*H*-azirines. Most computational modeling of this moiety has been performed using electronic structure methods where force fields are not needed, but which cannot characterize the processes at question in this work.[29–34] Some studies have used automatic parameter generation without adjustment.[17,34–36] We hope to address the limitations of

these studies by avoiding parameter assignment by pure analogy since there are few well-characterized and analogous moieties to carboxy-*2H*-azirines.[37,38]

Typical molecular dynamics simulations can fully characterize the behavior of molecular processes with timescales between 1 ps and 1 μs.[22,23,27] Because of the slow dynamics of membranes, straightforward atomistic simulations tend not to be able to reliably capture the equilibrium behavior of arbitrary small molecules relative to the bilayer.[22,23,39] However, enhanced sampling methods can overcome these limitations.[40,41] In these methods, the probability that configurations are sampled by the simulation is manipulated such that the full space of some *collective variable* (CV) is observed. A CV is a variable that summarizes the progress of some process of interest; the "reaction coordinate" is a similar concept specific to chemical reactions. Especially powerful are the enhanced sampling methods which allow for the reconstruction of the potential of mean force (PMF) with respect to the CV. The PMF can be used to calculate the free energy change associated with a process and so provide information about how likely the process is to occur under equilibrium conditions (i.e. *without* enhanced sampling).[42–44] Metadynamics is such a method.[45,46] Here, biases are added to the potential energy surface to encourage sampling of the collective variable; the accumulated biases can be used at the end of the simulation to reconstruct the potential of mean force.[45,46]

This work uses metadynamics as a tool to quantify the propensity of these carboxy-2*H*-azirine natural products to integrate in representative lipid bilayers. To accomplish this, we will obtain the PMF for moving the molecules into and out of the membrane. The PMF will allow us to calculate the free energy for membrane partitioning, thus determining if the molecules are thermodynamically stable in the membrane or aqueous solution. To distinguish between various possible interactions between the membrane and the molecules, we use the following definitions: a molecule broadly exhibiting "**binding**" is one which thermodynamically prefers *any* interaction with the membrane to simple solvation in ionized water; a molecule specifically exhibiting "**embedded binding**" is one which thermodynamically prefers to have its center buried within the hydrophobic lipid tails; a molecule specifically exhibiting "**peripheral binding**" is one which binds, but only *at or outside* the polar phosphate headgroups. We also investigate the orientation and solvent exposure of the molecules of interest by unbiasing the statistics from our biased simulations. These simulations will be performed for molecules **1**-*Z*-Dy-Me, **2**-*E*-Dy-Me, **6**-Az-H and two molecules known to exhibit membrane embedding: sphingosine (**7**-Sp) and stearic acid (**8**-St-H). This comparison will allow us to ensure that our metadynamics methods have properly ascertained the probability of embedded binding and allow us to determine if the physiochemical properties of our molecules are typical of membrane-embedding molecules.

In order to answer these questions, we developed a force field for the carboxy-*2H*-azirine moiety and an accessible metadynamics strategy with multiple convergence checks. These tools can be used to predict potential amphipathic behavior of compounds or natural product comprising poorly understood chemical moieties. More broadly, these studies with will allow us to infer if the mode of microbial inhibition of these carboxy-2*H*-azirine natural products is occurring with a biological target that is situated in, or near, the cell membrane lipid bilayer.

From the set of compounds used for this work, compounds **6**-Az-H and **8**-St-H have carboxyl groups, whereas **1**-Z-Dy-Me and **2**-E-Dy-Me have a methyl ester. Carboxyl groups are strongly hydrophilic and deprotonate in biological conditions (~pH 7.4) to yield carboxylates. Our work is focused on understanding the polarity of the carboxy-2*H*-azirine as a complete chemical

moiety. Performing our simulations with the deprotonated versions of **6**-Az-H and **8**-St-H risks simply confirming the strong hydrophilicity of carboxylates, rather than uncovering new information about the physiochemical properties of carboxy-2*H*-azirines in its entirety. As such, we performed simulations using the protonated versions of these moieties.

# Computational Methods

**Force Fields:** The CHARMM36 force field was used to model all molecular interactions.[28,47–49] However, force fields for molecules containing the carboxy-*2H*-azirine moiety are unavailable in CHARMM and the guesses obtained from CGenFF are highly unreliable (i.e. many penalties are much higher than 50).[50] In order to obtain reliable forcefields for this moiety, we first focused on one of the simplest azirines, 2*H*-azirine (i.e. $C_2H_3N$). To develop a CHARMM compatible force field, we used the program FFParam.[51] First, we used CGenFF to obtain initial force field parameters for 2*H*-azirine ($C_2H_3N$). The obtained charges were compared to a CHELPG charge analysis in Q-Chem 5.4 at MP2/6-31G*.[52,53] Note that while we should expect the general direction of the charges from the CHELPG analysis be similar to the final charges, we should not necessarily expect the absolute values to match. The fitted charges will specifically describe interactions with TIP3P water, and in CHARMM the charges of the H atoms are fixed. Most important in the comparison are three ideas: (1) the N should be less negative than CGenFF supposes, (2) the charge on the $sp^2$ hybridized C is does not need to be changed (additionally, the CGenFF penalty is < 50), and (3) the charge on $sp^3$ hybridized C should be negative, not positive. The CGenFF penalties were highest for the charges on the N and the $sp^3$ hybridized C, so we focused on fitting them. We optimized these atomic charges by fitting them to quantum mechanical energies (MP2/6-31G*) for interactions with TIP3P water, computed using Psi4 1.5.[48,54–56]

The bonding in 2*H*-azirine ($C_2H_3N$) is different from that of the molecules we actually intend to study. Thus, we parameterized **6**-Az-H as our minimal example of a 2*H*-azirine-containing molecule. After using CGenFF to obtain the initial force field, we observed that many of the high penalty interactions included the $sp^3$ carbon in the ring. Using constrained optimizations in Psi4 1.5 (for bonds and angles) and Q-Chem 5.4 (for dihedrals), we obtained potential energy surfaces for all high penalty (i.e. > 50) interactions except for dihedrals involving hydrogen, which FFParam does not recommend parameterizing.[51,53,54] These potential energy surfaces were obtained at the MP2/6-31G* level of electronic structure theory and all degrees of freedom besides the one being scanned were optimized at each step. All degrees of freedom were scanned starting from the optimized geometry. Bonds were scanned in 17 steps from 15 pm less than the optimized length to 15 pm more than the optimized length, and the optimized length was the central $9^{th}$ step. In a similar way, angles were scanned in 11 steps from 15 degrees below to 15 degrees above the optimum angle. For the dihedrals, full scans from -160 to 160 degrees were attempted. In several cases, only a portion of the potential energy surface could be collected due to high ring strain or interatomic clashes during optimization. However, the portion of the PES collected was always sufficient to fit the interaction of interest; the probability of the molecule exploring the un-scanned coordinate values in an ordinary 300 K MD simulation was negligible. Dihedrals were fit to the appropriate CHARMM sum-of-cosines functions, carefully monitoring how few could be used to

achieve a satisfactory fit of the potential energy surface. One out-of-plane improper dihedral angle was scanned from -5 to 5 degrees and fit to a harmonic interaction.

The charges for **6**-Az-H were obtained in the following way. First, CGenFF was used to obtain initial charges. As before, a CHELPG analysis (MP2/6-31G*) was used for guidance. Comparing the CGenFF penalties, the CHELPG analyses, and the charges obtained for 2*H*-azirine ($C_2H_3N$), we believed that the charges for the N and the $sp^3$ C in the ring would be similar between the two molecules. If the charge from 2*H*-azirine ($C_2H_3N$) for these atoms is used for **6**-Az-H, and the CGenFF values are used for all other charges, the overall charge is -0.209. According to CHELPG, the $sp^2$ carbon of **6**-Az-H could be expected to become more positive than in 2*H*-azirine ($C_2H_3N$), and CGenFF agrees with a penalty less than 50. The CGenFF penalty for the C in the carboxyl group, however, was greater than 50 and the CHELPG analysis implied that it should be more positive than CGenFF suggested. Thus, +0.209 units of charge were added to this atom. This leaves the overall molecule neutral. The final obtained point charges correlate well with synthetic observations of the electrophilicity and nucleophilicity of the atoms in *2H*-azirine bearing molecules.[57,58] The N and the ring $sp^3$ C are predicted to be nucleophilic, and the $sp^2$ C is predicted to be electrophilic.

The high penalty interactions for **1**-Z-Dy-Me and **2**-E-Dy-Me (which are stereoisomers and so have the same force field parameters) are the same as for **6**-Az-H, so the required force field parameters were simply borrowed. The initial (CGenFF) and final (FFParam) values of all the force field parameters and the CHELPG analyses are given in the SI. Some examples of how the coordinates of interest were scanned and fit will be provided on github at https://github.com/Daly-Lab-at-Haverford/code_examples.

**Molecular Dynamics Systems and Equilibration:** Initial structures of our small molecules embedded in a membrane were constructed using CHARMM-GUI's membrane builder.[59–62] The membrane bilayer was constructed from 75 % palmitoyloleoyl phosphatidylethanolamine (POPE) and 25 % palmitoyloleoyl phosphatidylglycerol (POPG) and was oriented so that its surface plane was aligned with the xy plane. This mixture has previously been used as an effective model of the inner bacterial membrane.[63] The x- and y-axis lengths of the membrane and the periodic box were initially 5 nm. Above and below the membrane 4 nm of water was added; NaCl was added to neutralize the membrane and then to a total ionic strength of 0.15 M. A distinct system was created for each molecule of interest and said molecule was initially placed in the center of the membrane. The structure of each molecule was initially obtained using Avogadro.[64] CHARMM-GUI was allowed to perform some initial minimization of the energy of the structure. The initial membrane structures with the molecules of interest inserted are shown in **Figure 4**.

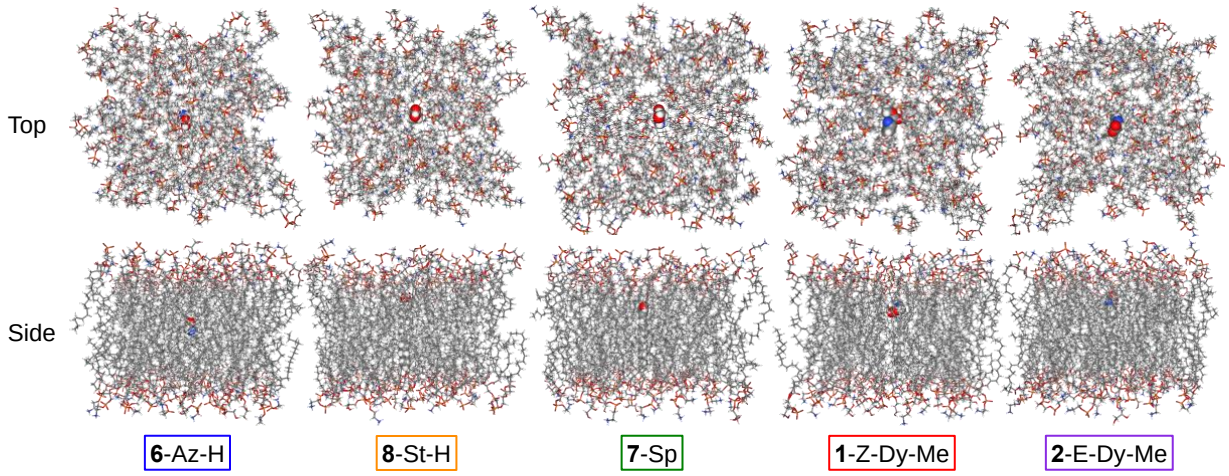


***Figure 4:*** *Initial structures of the molecule-embedded membrane prior to equilibration. Side and top views of the membrane are provided. Water and ions are not shown for clarity.*

The membrane systems taken from CHARMM-GUI were subjected to the equilibration procedure suggested by CHARMM-GUI and implemented in OpenMM 7.6.[65] The steps of this equilibration procedure have been outlined by Jo et al., though in the most recent version the $NP_z\gamma T$ (called NPAT in their work) simulation steps are each 500 ps.[60,66] To produce $NP_z\gamma T$ ensemble simulations, we held the surface tension ($\gamma$) at 0 kJ/mol/nm$^2$, the pressure in the z-axis direction ($P_z$) at 1 bar, and the temperature (T) at 300 K.[67] A Monte Carlo barostat with a update frequency of 150 steps was used to maintain the pressure and surface tension.[68] Temperatures were controlled using Langevin dynamics with a friction coefficient of 1 ps$^{-1}$.[69] All simulations were performed in this ensemble. Nonbonded interactions were cut off after 1.2 nm with a smooth switching function used from 1.0 nm. Long range electrostatics were corrected using Particle Mesh Ewald summation with an error tolerance of 0.0005. Configurations were sampled every 10 ps. After the equilibration recommended by CHARMM-GUI, velocities were randomized according to the Maxwell-Boltzmann distribution at 300 K and the system was equilibrated with no constraints for 2 ns.

**Well-Tempered Metadynamics:** PMFs were obtained using an OpenMM implementation of Well-Tempered Metadynamics.[46] In this method, biases are added to the system along a CV of interest, encouraging the system to explore the full range of values of the CV. As specific values of the CV are sampled, the strength of the biases added at those CV values is reduced. At long times (i.e. $t \to \infty$), the added biases will converge such that the bias along the CV stops changing. The total added bias is related to the PMF, $W(z)$,

$$W(z) = -\lim_{t\to\infty}\left[\frac{T+\Delta T}{\Delta T}V(z,t) + C(t)\right] \quad (1)$$

where $z$ is the CV, $T$ is the temperature of the simulation (300 K in this case), the biases are added in such a way that the CV is sampled as if the temperature was $T + \Delta T$, $V(z,t)$ is the total added bias as a function of $z$ and time, $t$, and $C(t)$ is a constant which can be ignored once convergence is reached.[46] In our simulations, $T + \Delta T = 6000$ K (i.e. the bias factor was 20). The CV was chosen to be the distance between the z-axis location of the center of mass of the

molecule of interest and the z-axis location of the center of mass of all POPE and POPG molecules (i.e. the central plane of the membrane). The biases were shaped as Gaussian functions with a standard deviation of 0.3 nm. The initial bias height was 25 kJ/mol and they were added every 100 fs. The CV was allowed to vary from -6 nm to 6 nm. This CV is visually depicted in **Figure 5**. Similar CVs and metadynamics settings have been used in previous studies of membrane embedding and partitioning.[70–72]

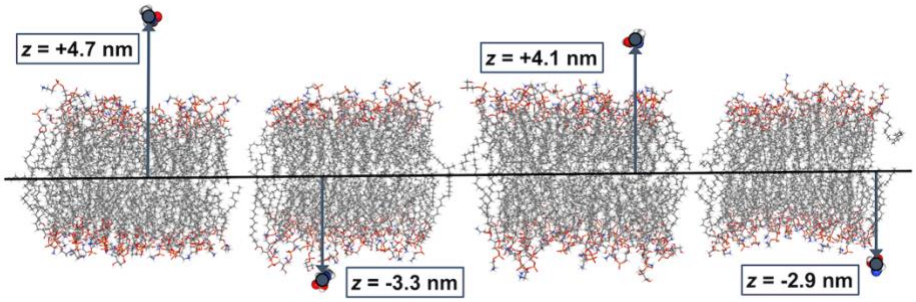


***Figure 5:*** *The collective variable explored by our metadynamics simulations is the distance between the central plane of the membrane and the center of mass of the molecule. Several snapshots from simulations of* ***6****-Az-H are used to exemplify this. Water and ions are not shown for clarity. All collective variable values are in nm.*

Because of the symmetry of the system, the PMF should be even i.e. $W(z) = W(-z)$. Metadynamics simulations were run for 2 μs and then continued in 500 ns increments until three criteria were met: (1) the RMSD between $W(z)$ and $W(-z)$ was at most 4 kJ/mol for any specific value of $z$ ; (2) the RMS standard error over *all* values of $z$ between $W(z)$ and $W(-z)$ was below 2.5 kJ/mol; and (3) the RMSD between the potential of mean force obtained at the end of the simulation and that obtained 50 ns prior to the end was less than 2.5 kJ/mol across all values of $z$. This took different amounts of simulation time for each molecule (**Table 1**). Due to these criteria, the ones place is treated as the final significant place value in the free energy values obtained in this work.

***Table 1:*** *The time to convergence for each metadynamics simulation.*

| Molecule | Time (μs) |
|---|---|
| **6**-Az-H | 2.0 |
| **8**-St-H | 2.0 |
| **7**-Sp | 4.0 |
| **1**-Z-Dy-Me | 3.0 |
| **2**-E-Dy-Me | 2.0 |

Metadynamics simulations were run under $NP_z\gamma T$ conditions (1 bar, 0 kJ/mol/nm$^2$, 300 K). After our simulations converged, we used the reweighting method of Branduardi et al. to weight the statistics of the simulation configurations observed under metadynamics.[73] The unbiased probability, $P_u(\boldsymbol{r})$, of a given simulation configuration $\boldsymbol{r}$ (representing all atomic positions) is given by,

$$P_u(\boldsymbol{r}) = P_b(\boldsymbol{r})e^{+\beta V(z(\boldsymbol{r}),t\to\infty)} \quad (2)$$

where $z(\boldsymbol{r})$ is the value of the CV in the configuration $\boldsymbol{r}$ of interest, $P_b(\boldsymbol{r})$ is the biased probability with which the configuration was observed under metadynamics, $V(z(\boldsymbol{r}), t \to \infty)$ is the converged bias surface, and $\beta = \frac{1}{k_b T}$.[73,74] The quantity $e^{\beta V(z(\boldsymbol{r}),t\to\infty)}$ can be thought of as a weighting factor which removes the effect of the bias potential, leaving only the original free energy surface to affect configurational probabilities. However, using metadynamics has allowed for the sampling of configurations across $z$ even if their unbiased probability was marginal, allowing for more complete statistics.

# Results

### Potentials of Mean Force and Binding Free Energies:

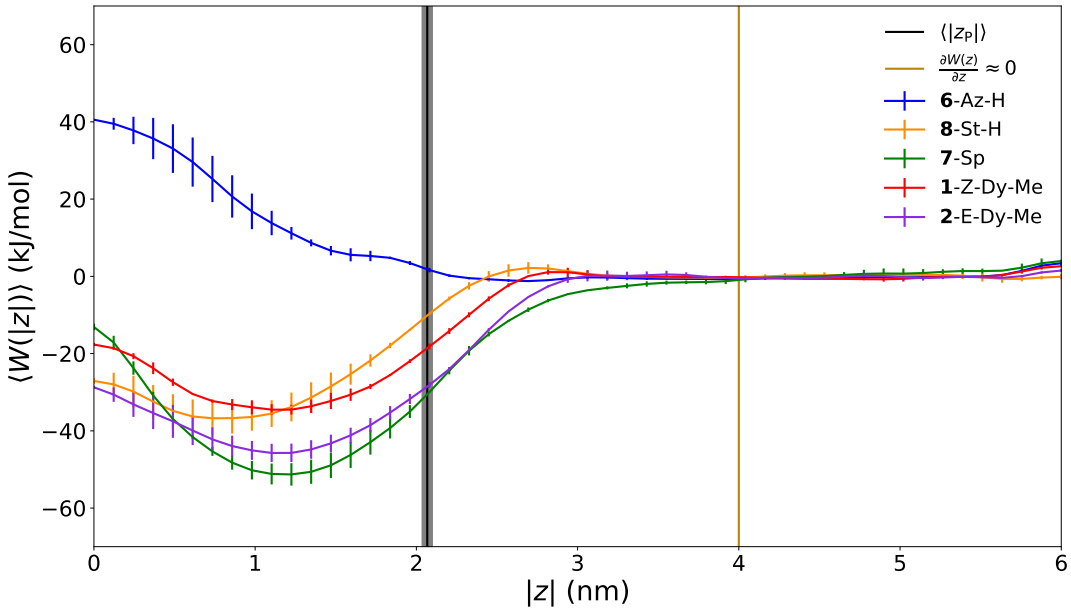


***Figure 6:*** *Potentials of mean force for the z-axis distance between the membrane center and the center of mass of the molecule of interest. Values are averages between* $W(z)$ and $W(-z)$ *and error bars are 95 % confidence intervals. For comparison, the average location of the membrane phosphate groups is shown in black and the standard deviation of this average is shown as a grey "spread." The zero of energy in this plot is the average value in the unbound region (*$|z| \geq 4$*).*

We divide the space across the simulated lipid bilayer into three regions to facilitate describing interactions between our molecules of interest and the membrane. (1) Relatively far from the bilayer, molecules are *unbound*, meaning that the membrane has no influence on their

behavior. Here, we define the unbound region to be that part of the PMF where $\frac{dW(z)}{dz} \approx 0$ as would be expected for a non-interacting molecule.[42,71] This region was chosen to be where $|z| \geq 4$. The exact value of the cutoff is flexible, as the lowest points on the PMF make the largest contributions to the free energy calculations described below. Molecules which are not in this region are in the *bound region*. (2) A molecule inside the membrane would be exhibiting *embedded binding*. Values of the CV with absolute value smaller than $\langle |z_{\mathrm{P}}| \rangle$, the average distance of membrane phosphate atoms from the membrane center of mass (about 2.07 nm), are considered to be inside the embedded binding region. (3) Nearer to but still outside the membrane, the molecules can be *peripherally bound*. The peripheral binding region is the bound region but without the embedded binding region i.e. $\sim 2.07 < |z| \leq 4$.

Under these definitions, there are several processes of interest to our work. First, a molecule could move from the unbound region to the bound region; the associated free energy change is $\Delta G_{\mathrm{b}}$. A molecule could move from the unbound region to the peripheral binding region; the associated free energy change is $\Delta G_{\mathrm{u}\to\mathrm{pb}}$. Additionally, a molecule could move from the peripheral binding region to the embedded binding region; the associated free energy change is $\Delta G_{\mathrm{pb}\to\mathrm{eb}}$. We can combine these last two free energies to obtain the free energy associated with moving from the unbound region to the embedded binding region, $\Delta G_{\mathrm{u}\to\mathrm{eb}}$, which is the value we are most concerned with, using,

$$\Delta G_{\mathrm{u}\to\mathrm{eb}} = \Delta G_{\mathrm{u}\to\mathrm{pb}} + \Delta G_{\mathrm{pb}\to\mathrm{eb}} \tag{3}$$

The terms on the right side of this equation can be obtained directly from the PMFs shown in Figure 6. The free energy change for moving from the unbound region to the peripheral binding region is

$$\Delta G_{\mathrm{u}\to\mathrm{pb}} = -\beta^{-1} \ln \left[ \frac{\int_{\mathrm{pb}} e^{-\beta W(z)} dz}{\int_{\mathrm{u}} e^{-\beta W(z)} dz} \right] \tag{4}$$

The symbols in this equation retain their prior meanings. The integral in the numerator is over the peripherally bound region signified by $\mathrm{pb}$ and the integral in the denominator is over the unbound region signified by $\mathrm{u}$. Similarly, the free energy for moving from the peripheral binding region to the embedded binding region is

$$\Delta G_{\mathrm{pb}\to\mathrm{eb}} = -\beta^{-1} \ln \left[ \frac{\int_{\mathrm{eb}} e^{-\beta W(z)} dz}{\int_{\mathrm{pb}} e^{-\beta W(z)} dz} \right] \tag{5}$$

Plugging these expressions into Eq. 3, we obtain

$$\Delta G_{\mathrm{u}\to\mathrm{eb}} = -\beta^{-1} \ln \left[ \frac{\int_{\mathrm{eb}} e^{-\beta W(z)} dz}{\int_{\mathrm{u}} e^{-\beta W(z)} dz} \right] \tag{6}$$

We also computed free energies changes for general binding from the PMFs,

$$\Delta G_{\mathrm{b}} = -\beta^{-1} \ln \left[ \frac{\int_{\mathrm{b}} e^{-\beta W(z)} dz}{\int_{\mathrm{u}} e^{-\beta W(z)} dz} \right] \tag{7}$$

where the integral in the numerator is over the entire bound region signified by $\mathrm{b}$. These free energy changes can be found in Table 2.

The PMFs and free energy changes obtained using these methods clearly show that all the molecules of interest exhibit general binding to the membrane. However, **6**-Az-H is clearly distinct from the other molecules. **6**-Az-H is essentially indifferent to the choice between the unbound and peripheral regions, but it will not display embedded binding. The other molecules all strongly prefer to embed within the membrane over all other possibilities. Comparing $\Delta G_{\mathrm{b}}$, $\Delta G_{\mathrm{u}\to\mathrm{eb}}$, and $\Delta G_{\mathrm{u}\to\mathrm{pb}}$, we see that the thermodynamics of general binding is strongly dominated by the more favorable sub-binding process.

***Table 2:*** *The free energies obtained for the interactions of the molecules of interest with the membrane in kJ/mol. Free energy values are in kJ/mol. Values are rounded to the ones digit.*

| **Molecule** | $\boldsymbol{\Delta G_{\mathrm{b}}}$ | $\boldsymbol{\Delta G_{\mathrm{u}\to\mathrm{pb}}}$ | $\boldsymbol{\Delta G_{\mathrm{pb}\to\mathrm{eb}}}$ | $\boldsymbol{\Delta G_{\mathrm{u}\to\mathrm{eb}}}$ |
|---|---|---|---|---|
| **6**-Az-H | 0 | 0 | +8 | +8 |
| **8**-St-H | -36 | -4 | -32 | -36 |
| **7**-Sp | -49 | -24 | -26 | -49 |
| **1**-Z-Dy-Me | -32 | -12 | -20 | -32 |
| **2**-E-Dy-Me | -43 | -22 | -22 | -43 |

**Binding Probability and Orientation:**

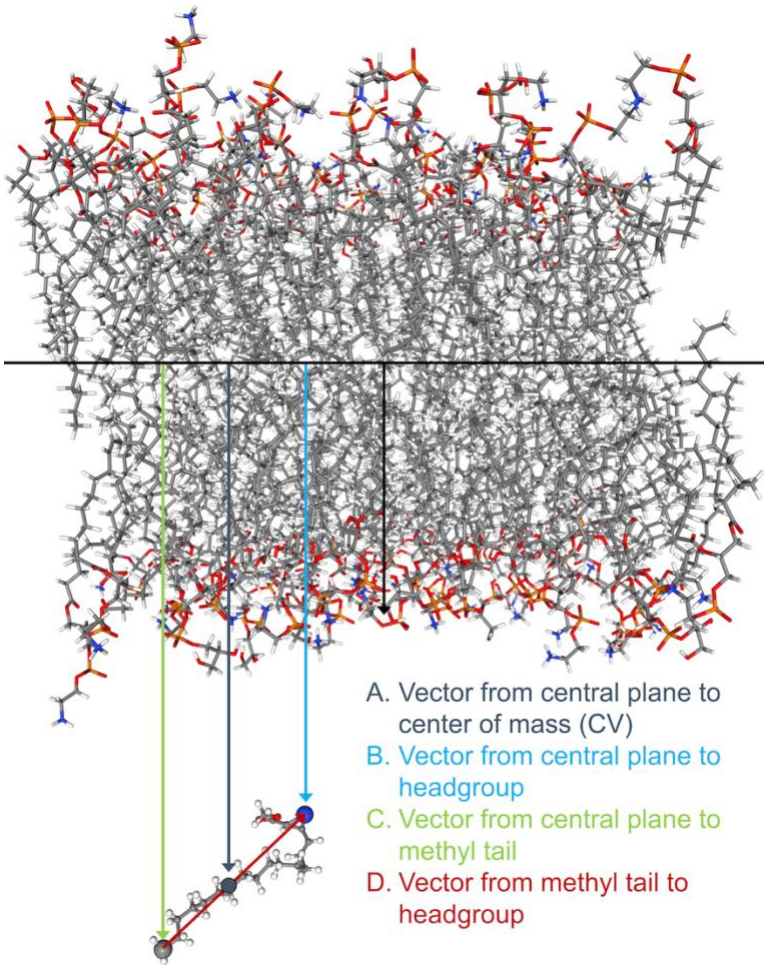


***Figure 7:*** *Vectors used to define the unbiased probability distributions shown in* ***Figure 8****. The letters used in this figure correspond with the letters in* ***Figure 8****. The pictured molecule of interest is* ***2****-E-Dy-Me and water and ions have been removed for clarity. Per the results shown below, the pictured configuration is highly unlikely in the real system.*

The structural relationship between our molecules and the membrane is vitally important. It is not sufficient to know that a carboxy-2*H*-azirine-bearing molecule embeds within the membrane. We must also ask if the carboxy-2*H*-azirine group itself is available for further biological interactions. This question was addressed by computing the unbiased probability density for configurations of interest. Four types of analysis were performed, and they are based on vectors depicted in **Figure 7**. The results of these analyses are shown in **Figure 8**. The first, in **Figure 8A**, is to compute the unbiased probability of the absolute value of the CV, which is the z-axis distance between the center of mass of the membrane and the center of mass of the molecule of interest. Except for **6**-Az-H, the molecules are most likely to become embedded in the membrane (also see **Figure 6**). Notice that **6**-Az-H has a small peak just above the membrane's phosphate groups at about 2.5 nm. This is an indication of weak peripheral binding to the surface of the membrane. The probability is peaked around 1 nm for the other molecules, well inside the membrane. Another interesting feature which is only visible for **6**-Az-H is a decrease in the probability above about 5.5 nm. This likely arises from the constant pressure

control in the z-dimension; there were many configurations where the box was slightly smaller than 12 nm, so distances near 6 nm were unphysically less likely to be achieved. This has no effect on the major results of this work.

The second type of analysis focused on the headgroups of the molecules of interest. For **6**-Az-H, **2**-E-Dy-Me, and **1**-Z-Dy-Me, the headgroup was represented by the N atom. For **7**-Sp and **8**-St-H, an O atom was selected. The probability distribution of these atoms is shown in **Figure 8B**. As expected, the distribution for **6**-Az-H is close to zero inside the membrane. For the other molecules, the peaks of the headgroup probabilities cluster around 1.5 nm, with significant density protruding beyond the membrane's phosphorous headgroups. The portion of probability density outside the membrane and the average distance of the protruding headgroup is quantified in **Table 3**. The total protruding probability, $P_p$, is given by

$$P_p = \int_{\langle |z_P| \rangle}^{6} P_u(d_z) dd_z \tag{8}$$

where $d_z$ is the z-axis distance from the central plane of the membrane. The average protruding distance, $\langle d_{z,p} \rangle$, is

$$\langle d_{z,p} \rangle = \int_{\langle |z_P| \rangle}^{6} (d_z - \langle |z_P| \rangle) P_u(d_z) dd_z \tag{9}$$

The **2**-E-Dy-Me and **1**-Z-Dy-Me headgroup exposure probabilities and protruding distances are centered between the same values for **7**-Sp and **8**-St-H. **6**-Az-H is mostly outside the membrane.

***Table 3:*** *The portion of headgroup probability density and the average distance the headgroups protrude outside the membrane phosphate groups. Note that the protruding distance is in Å (not nm) for clarity.*

| Molecule | $P_p$ | $\langle d_{z,p} \rangle$ (Å) |
|---|---|---|
| **6**-Az-H | 0.966 | 17.6 |
| **8**-St-H | 0.018 | 0.0 |
| **7**-Sp | 0.19 | 0.2 |
| **1**-Z-Dy-Me | 0.07 | 0.1 |
| **2**-E-Dy-Me | 0.05 | 0.1 |

Third, we examined the methyl tails. For all our molecules of interest, the final C in the carbon chain was selected to represent the tail end of the molecule. For **6**-Az-H, this was the C in the methyl tail off the azirine ring. In **Figure 8C** these distributions are peaked at 0 nm for all molecules except **6**-Az-H. It should be noted that the **6**-Az-H distributions are nearly identical between all three distance-based methods of analysis, implying that its orientation is not fixed. For the other molecules, there is nearly no methyl tail probability density above 1 nm.

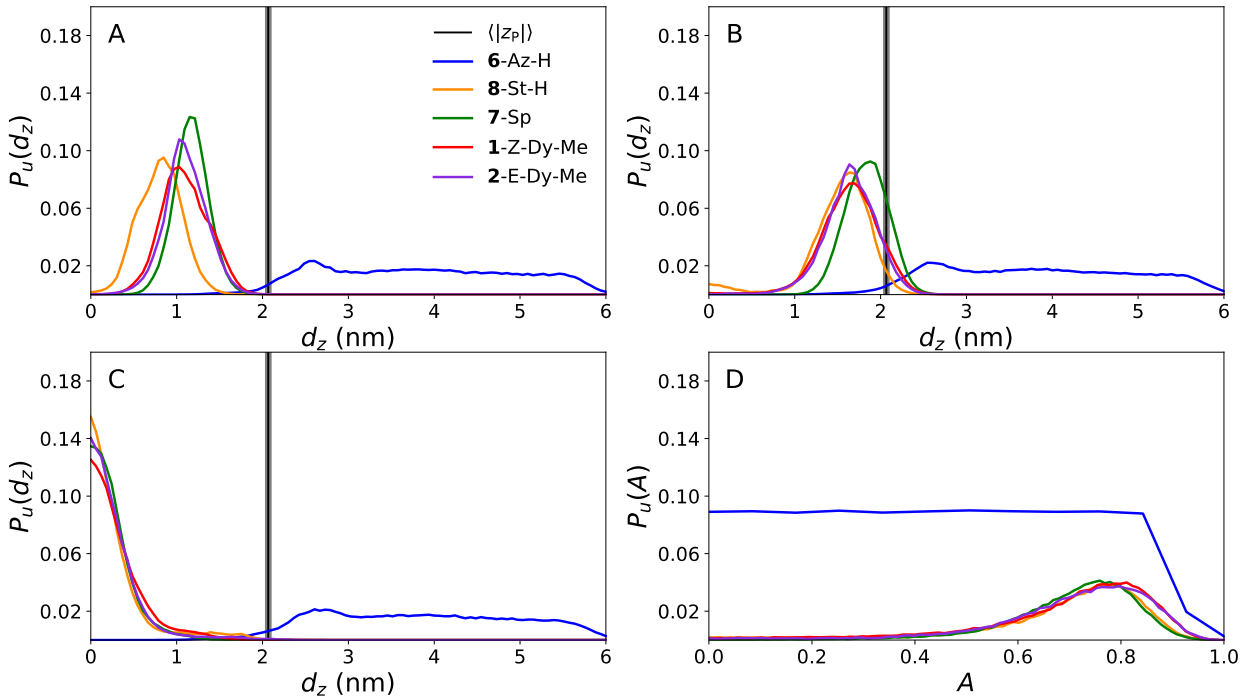


***Figure 8:*** *The unbiased probability density for the z-axis distance, $d_z$, for the (A) center of mass for each molecule, (B) headgroup atom, or (C) methyl tail C atom from the center of mass of the membrane. For comparison, the average location of the membrane phosphate groups is shown in black and the standard deviation of this average is shown as a grey "spread." (D) The alignment of the vector connecting the headgroup and methyl tail atoms with the membrane.*

The above results already strongly imply that the molecules **1**-*Z*-Dy-Me, **2**-*E*-Dy-Me, and **7**-Sp, **8**-St-H are embedded in the membrane and are oriented with their headgroups pointed towards the solvent and with their methyl tails pointed into the center of the membrane. To confirm this, we computed a direct measure of alignment with the membrane bilayer. We assumed that the membrane surface normal unit vector was always identical to the z-axis unit vector, $\hat{z}$ . Then, we defined the alignment, $A$ as,

$$A = \frac{\left| \hat{z} \cdot \vec{l} \right|}{\sqrt{\mathrm{Max}\left( \vec{l} \cdot \vec{l} \right)}} \tag{10}$$

where $\vec{l}$ is the vector pointing from the methyl tail to the headgroup atom in a particular molecule. The denominator of Equation 10 is the maximum molecule length ever observed in our simulations. Our metadynamics simulations sample a wide variety of molecular configurations, so this is an effective proxy for the length of each molecule at full elongation. The numerator is the length of the molecule in a specific configuration, but only in the z-axis direction. When $A = 1$, the molecule is fully elongated *and* is perfectly aligned with the z-axis. In other words, $A = 1$ describes perfect alignment with a single leaflet of the membrane. The $A = 0$ endpoint can describe several possibilities. For instance, the molecule could be completely elongated, but have a 90° angle with respect to the membrane surface normal. Alternatively, $A$ will be close to zero if the molecule has a small radius of gyration. In any case, values $A$ near zero describe a distinct *lack* of alignment

with the membrane. The unbiased probability distribution of alignment values observed in our simulations is given in **Figure 8D**. The results clearly show that all molecules of interest are most often aligned with the membrane except **6**-Az-H. All alignments for **6**-Az-H are equally probable, as would be expected from the results shown in **Figure 8A-C**. The probability of alignments especially close to 1 is somewhat depressed because the largest molecular lengths require bond elongation which is generally energetically unfavorable.

# Discussion

In the fight against antimicrobial resistance, the importance of drug innovation cannot be overstated. The most sustainable approach to mitigating antimicrobial resistance relies on the development of structurally innovative inhibitors that function through a unique mechanism of action and so circumvent any current resistance mechanisms. The carboxy-2*H*-azirine moiety first emerged as a unique scaffold for microbial inhibition when azirinomycin (**6**-Az-H) was isolated in 1971 from a soil bacterial strain of *Streptomyces aureus*.[8] Stapley *et al*. screened the antibacterial properties of **6**-Az-H against numerous common bacterial strains with a disk diffusion assay and found broad inhibitory activity.[2] In subsequent years additional carboxy-2*H*-azirine natural products were discovered (**1** – **5**).[3–7] Skepper *et al*. reported the *in vitro* $MIC_{50}$ of **1**-*Z*-Dy-Me against many fluconazole resistant fungal strains ($MIC_{50}$ of compound **1**-*Z*-Dy-Me reported as 4 µg/mL for *Candida albicans* 96-489 and *Candida krusei*),[3] Keffer *et al*. reported inhibition of the free acid of **3a**-E-An-Me with *Staphylococcus aureus* and methicillin-resistant *S. aureus* (MRSA) ($MIC_{50}$ of **3a**-E-An-Me reported as 1.2 µg/mL for *S. aureus*, and 9.3 µg/mL with MRSA)[4].

Despite these intriguing inhibition results, the biological target of inhibition is currently unknown. The carboxy-2*H*-azirine is a unique and understudied moiety and its structure does not readily inspire confident assumptions about physiological behavior. To clarify the properties of this moiety and begin to build an understanding of antimicrobial activity, we set out to predict the membrane partitioning behavior of molecules with a carboxy-2*H*-azirine functional group in a lipid bilayer. This includes investigating the orientation of these molecules when embedded in a lipid bilayer, as well as how these molecules protrude in relation to the polar phosopholipid head groups of the lipid bilayer.

This work was performed with compounds **1**-*Z*-Dy-Me, **2**-*E*-Dy-Me, and **6**-Az-H as representatives of the natural product carboxy-2*H*-azirine set. We selected **1**-*Z*-Dy-Me and **2**-*E*-Dy-Me because these compounds are geometric isomers, and such structural differences are known to impact membrane-dependent cell functions by altering membrane fluidity.[75,76] Thus, membrane embedding may be expected to differ between these two isomers, possibly leading to distinct mechanisms of inhibition. Comparing the long, straight-chain, alkyl compounds composed of an 18-carbon chain, **1**-*Z*-Dy-Me, **2**-*E*-Dy-Me, **7**-Sp, **8**-St-H, against a short alkyl chain compound composed of a 4-carbon chain, **6**-Az-H allowed us to investigate the effect of carbon chain length on membrane embedding. Long alkyl chains in small molecule inhibitors can be distinct drivers of membrane integration,[77] but the alkyl chain length and chain saturation can also influence binding affinity with a membrane-bound molecular target.[78,79] We sought to identify any perturbations the carboxy-2*H*-azirine could have on the ability of long-chain molecules to embed in a membrane. Finally, recognizing if the carboxy-2*H*-azirine will protrude past the lipid phosphate headgroups, or if the moiety will sink below the bilayer, can be crucial for correlating proximity to a structurally

characterized potential membrane target. Thus, when embedded, we compared orientation of these molecules with respect to the phosphates of the lipid bilayer. We expect these long chain carboxy-2*H*-azirines to preferentially orient parallel with the lipid bilayer with the carboxy-2*H*-azirine pointed towards the polar lipid head groups. If these molecules were found to orient in any unexpected direction, then passive diffusion may be possible, thus expanding the possible inhibition targets.

***Table 4:*** *Summary of results. The binding depth is the average center of mass distance of each molecule from the membrane phosphate groups. The molecular angle is the average angle between the z-axis and the vector connecting the tail and head of each molecule. The average of 90° for* ***6****-Az-H is not an indication that it is typically orthogonal to the membrane. Instead, the molecule adopts all angles from 0° to 180° equally. The protruding distance is the maximum distance from the membrane phosphate groups where there is at least a 1 % chance of observing the headgroup.*

| Molecule | Binding Depth (nm) | Molecular Angle (degrees) | Protruding Distance (nm) |
|---|---|---|---|
| **6**-Az-H | +1.75 | 90.00 | 3.62 |
| **8**-St-H | -1.26 | 37.2 | 0.05 |
| **7**-Sp | -0.89 | 35.5 | 0.25 |
| **1**-Z-Dy-Me | -0.97 | 38.2 | 0.17 |
| **2**-E-Dy-Me | -0.97 | 36.6 | 0.17 |

We have provided a summary of our results in Table 4. Our results strongly predict that, at equilibrium, molecules **8**-St-H, **7**-Sp, **1**-Z-Dy-Me, and **2**-E-Dy-Me will display embedded binding to a lipid membrane while **6**-Az-H will not. Even this exceptional molecule may display peripheral binding (**Figure 8**). Moving from an unbound state to a peripheral binding state is always favorable and, except for **6**-Az-H, moving from a peripheral binding state to an embedded binding state is also favorable. For molecules **8**-St-H, **7**-Sp, **1**-Z-Dy-Me, and **2**-E-Dy-Me, the reverse processes of moving from embedded binding to the unbound state or from embedded binding to peripheral binding are both highly unfavorable and essentially will never be observed in experiment. The large free energy changes observed in this study give us the confidence to predict that embedded membrane binding processes will remain favorable for molecules **8**-St-H, **7**-Sp, **1**-Z-Dy-Me, and **2**-E-Dy-Me even if the composition of the membrane is changed substantially from our particular mixture of 75 % POPE and 25 % POPG.

We also predict that the carboxy-2*H*-azirine moiety is sufficiently hydrophilic to act in much the same way as the amino and carboxy groups present in **7**-Sp and **8**-St-H, respectively. The charge distribution in our force field, supported by quantum chemical CHELPG population analysis, is consistent with other hydrophilic compounds. The charges adopted for the N (-0.357) and the $sp^2$ C (+0.427) in the 2*H*-azirine ring are similar in magnitude to those of the H atoms in TIP3P water (+0.417). We also find that **6**-Az-H, the smallest carboxy-2*H*-azirine natural product strongly prefers aqueous solution to the hydrophobic space within the membrane. The *2H*-azirine groups in **2**-E-Dy-Me, and **1**-Z-Dy-Me also prefer aqueous solution, causing these molecules to orient with those moieties facing the water layer and to protrude slightly beyond the phosphate

head groups in the membrane. This behavior is similar to that observed for **7**-Sp and **8**-St-H. Like these non-azirine-containing compounds, the hydrophobic tails of **2**-E-Dy-Me, and **1**-Z-Dy-Me point towards the center of the membrane and align parallel with the membrane.

# Conclusions

Currently, biochemical validation of these studies is hampered by the synthetic feasibility of generating enough material for comprehensive microbial assays with the complete panel of carboxy-2*H*-azirine natural products. This computational work served as a valuable first step to allow us to make tentative predictions about potential biological targets for carboxy-2*H*-azirine inhibition based on membrane embedding behaviors, ultimately guiding the start of experimental validation. This work has guided our first steps towards a protein-centric investigation for uncovering the biological targets of the carboxy-2*H*-azirine natural products. Proteins exhibit diverse structures and functions which allows for the complex structures of natural products to interact through numerous binding modes, allowing for high affinity binding.[80]

With regards to a protein-focused investigation of these carboxy-2*H*-azirine compounds, it is clear from our metadynamics simulations that **6**-Az-H is an expected outlier, and must be separately investigated. Lacking a long alkyl chain, **6**-Az-H demonstrates complete aqueous partitioning due to the isolated hydrophilicity with the minimal carboxy-2*H*-azirine scaffold. This mode of binding suggests a distinct mechanism of action compared to those with longer alkyl chains; for instance, **6**-Az-H may target a soluble or a membrane embedded process. In contrast, the membrane embedding for **1**-Z-Dy-Me and **2**-E-Dy-Me suggests that the whole set of long alkyl chain analogs (**1**-**5**) may exclusively target biological processes at, or near, the lipid membrane.

In this work, we have made predictions of the membrane partitioning of carboxy-2*H*-azirine containing molecules and determined that the moiety itself is likely hydrophilic, similar to an amino or hydroxyl group. We utilize an oversimplified model membrane that does not account for the complexities found in real membrane environments. Membrane complexities encompass phospholipids, cholesterol, proteins, and carbohydrates that gives the membrane a fluid character.[81] However, even in our simplified representation, we see the same behavior between molecules that are known to embed in realistic membranes (**7**-Sp and **8**-St-H) and **2**-E-Dy-Me, and **1**-Z-Dy-Me. This and the large free energy changes upon embedding we observe give us confidence that our results apply to systems containing all the complexity we've removed. Like other long chain molecules, the mixture of polar and non-polar interactions leads to long-chain molecules embedding in lipid bilayers with the hydrophilic carboxy-2*H*-azirine group co-located with the polar phospholipid headgroups of the membrane bilayer. Gaining this understanding of the physiochemical properties of carboxy-2H-azirines utilizing metadynamics has been a crucial first step for elucidating the biological mechanisms of inhibition of these molecules. Moreover, such understanding opens up this unexplored chemical space, offering a distinct scaffold with promising potential for therapeutic development.

# Supporting Information Description

Included in the supporting information files are the initial CGenFF force field files for all of the small molecules, Q-Chem output files containing CHELPG analyses of 2*H*-azirine and **6**-Az-H, and the final force field files obtained using FFParam. These are all provided as text files.

# Acknowledgments

Computational resources were provided in part by the MERCURY consortium (https://mercuryconsortium.org/) under NSF grants CHE-1229354, CHE-1662030, and CHE-2018427. C.A.D. and L.S. also thank Haverford College for startup funding and computational resources.

# References

(1) Butler, M. S.; Blaskovich, M. A.; Cooper, M. A. Antibiotics in the Clinical Pipeline in 2013. *J Antibiot* **2013**, *66* (10), 571–591. https://doi.org/10.1038/ja.2013.86.
(2) Stapley, E. O.; Hendlin, D.; Jackson, M.; Miller, A. K.; Hernandez, S.; Mata, J. M. Azirinomycin. I. Microbial Production and Biological Characteristics. *J Antibiot (Tokyo)* **1971**, *24* (1), 42–47.
(3) Skepper, C. K.; Dalisay, D. S.; Molinski, T. F. Synthesis and Antifungal Activity of (−)-( *Z* )-Dysidazirine. *Org. Lett.* **2008**, *10* (22), 5269–5271. https://doi.org/10.1021/ol802065d.
(4) Keffer, J. L.; Plaza, A.; Bewley, C. A. Motualevic Acids A−F, Antimicrobial Acids from the Sponge *Siliquariaspongia* Sp. *Org. Lett.* **2009**, *11* (5), 1087–1090. https://doi.org/10.1021/ol802890b.
(5) Skepper, C. K.; Molinski, T. F. Long-Chain 2 *H* -Azirines with Heterogeneous Terminal Halogenation from the Marine Sponge *Dysidea Fragilis*. *J. Org. Chem.* **2008**, *73* (7), 2592–2597. https://doi.org/10.1021/jo702435s.
(6) Molinski, T. F.; Ireland, C. M. Dysidazirine, a Cytotoxic Azacyclopropene from the Marine Sponge Dysidea Fragilis. *J. Org. Chem.* **1988**, *53* (9), 2103–2105. https://doi.org/10.1021/jo00244a049.
(7) Gunasekera, S. P.; Kokkaliari, S.; Ratnayake, R.; Sauvage, T.; Dos Santos, L. A. H.; Luesch, H.; Paul, V. J. Anti-Inflammatory Dysidazirine Carboxylic Acid from the Marine Cyanobacterium Caldora Sp. Collected from the Reefs of Fort Lauderdale, Florida. *Molecules* **2022**, *27* (5), 1717. https://doi.org/10.3390/molecules27051717.
(8) Miller, T. W.; Tristram, E. W.; Wolf, F. J. Azirinomycin. II. Isolation and Chemical Characterization as 3-Methyl-2(2H) Azirinecarboxylic Acid. *J Antibiot (Tokyo)* **1971**, *24* (1), 48–50.
(9) Yin, H.; Flynn, A. D. Drugging Membrane Protein Interactions. *Annu. Rev. Biomed. Eng.* **2016**, *18* (1), 51–76. https://doi.org/10.1146/annurev-bioeng-092115-025322.
(10) Atkovska, K.; Klingler, J.; Oberwinkler, J.; Keller, S.; Hub, J. S. Rationalizing Steroid Interactions with Lipid Membranes: Conformations, Partitioning, and Kinetics. *ACS Cent. Sci.* **2018**, *4* (9), 1155–1165. https://doi.org/10.1021/acscentsci.8b00332.
(11) King, J. P.; Wang, A. Putative Roles of Terpenoids in Primitive Membranes. *Frontiers in Ecology and Evolution* **2023**, *11*.

(12) Hakulinen, J. K.; Hering, J.; Brändén, G.; Chen, H.; Snijder, A.; Ek, M.; Johansson, P. MraY–Antibiotic Complex Reveals Details of Tunicamycin Mode of Action. *Nat Chem Biol* **2017**, *13* (3), 265–267. https://doi.org/10.1038/nchembio.2270.
(13) Hering, J.; Dunevall, E.; Snijder, A.; Eriksson, P.-O.; Jackson, M. A.; Hartman, T. M.; Ting, R.; Chen, H.; Price, N. P. J.; Brändén, G.; Ek, M. Exploring the Active Site of the Antibacterial Target MraY by Modified Tunicamycins. *ACS Chem. Biol.* **2020**, *15* (11), 2885–2895. https://doi.org/10.1021/acschembio.0c00423.
(14) Patil, A.; Majumdar, S. Echinocandins in Antifungal Pharmacotherapy. *Journal of Pharmacy and Pharmacology* **2017**, *69* (12), 1635–1660. https://doi.org/10.1111/jphp.12780.
(15) Szymański, M.; Chmielewska, S.; Czyżewska, U.; Malinowska, M.; Tylicki, A. Echinocandins – Structure, Mechanism of Action and Use in Antifungal Therapy. *Journal of Enzyme Inhibition and Medicinal Chemistry* **2022**, *37* (1), 876–894. https://doi.org/10.1080/14756366.2022.2050224.
(16) Khlebnikov, A. F.; Novikov, M. S.; Rostovskii, N. V. Advances in 2H-Azirine Chemistry: A Seven-Year Update. *Tetrahedron* **2019**, *75* (18), 2555–2624. https://doi.org/10.1016/j.tet.2019.03.040.
(17) Ma, N.; Hu, J.; Zhang, Z.-M.; Liu, W.; Huang, M.; Fan, Y.; Yin, X.; Wang, J.; Ding, K.; Ye, W.; Li, Z. 2H-Azirine-Based Reagents for Chemoselective Bioconjugation at Carboxyl Residues Inside Live Cells. *J. Am. Chem. Soc.* **2020**, *142* (13), 6051–6059. https://doi.org/10.1021/jacs.9b12116.
(18) Anderson, A. J.; Seebald, L. M.; Arbour, C. A.; Imperiali, B. Probing Monotopic Phosphoglycosyl Transferases from Complex Cellular Milieu. *ACS Chem. Biol.* **2022**, *17* (11), 3191–3197. https://doi.org/10.1021/acschembio.2c00648.
(19) Skepper, C. K.; Dalisay, D. S.; Molinski, T. F. Synthesis and Chain-Dependent Antifungal Activity of Long-Chain 2H-Azirine-Carboxylate Esters Related to Dysidazirine. *Bioorganic & Medicinal Chemistry Letters* **2010**, *20* (6), 2029–2032. https://doi.org/10.1016/j.bmcl.2010.01.068.
(20) Carter, H. E.; Glick, F. J.; Norris, W. P.; Phillips, G. E. BIOCHEMISTRY OF THE SPHINGOLIPIDES. *Journal of Biological Chemistry* **1947**, *170* (1), 285–294. https://doi.org/10.1016/S0021-9258(17)34955-4.
(21) Hannun, Y. A.; Obeid, L. M. Sphingolipids and Their Metabolism in Physiology and Disease. *Nat Rev Mol Cell Biol* **2018**, *19* (3), 175–191. https://doi.org/10.1038/nrm.2017.107.
(22) Marrink, S. J.; Corradi, V.; Souza, P. C. T.; Ingólfsson, H. I.; Tieleman, D. P.; Sansom, M. S. P. Computational Modeling of Realistic Cell Membranes. *Chem. Rev.* **2019**, *119* (9), 6184–6226. https://doi.org/10.1021/acs.chemrev.8b00460.
(23) Enkavi, G.; Javanainen, M.; Kulig, W.; Róg, T.; Vattulainen, I. Multiscale Simulations of Biological Membranes: The Challenge To Understand Biological Phenomena in a Living Substance. *Chem. Rev.* **2019**, *119* (9), 5607–5774. https://doi.org/10.1021/acs.chemrev.8b00538.
(24) Shinoda, W. Permeability across Lipid Membranes. *Biochimica et Biophysica Acta (BBA) - Biomembranes* **2016**, *1858* (10), 2254–2265. https://doi.org/10.1016/j.bbamem.2016.03.032.
(25) Venable, R. M.; Krämer, A.; Pastor, R. W. Molecular Dynamics Simulations of Membrane Permeability. *Chem. Rev.* **2019**, *119* (9), 5954–5997. https://doi.org/10.1021/acs.chemrev.8b00486.
(26) Hannesschlaeger, C.; Horner, A.; Pohl, P. Intrinsic Membrane Permeability to Small Molecules. *Chem. Rev.* **2019**, *119* (9), 5922–5953. https://doi.org/10.1021/acs.chemrev.8b00560.

(27) Leach, A. R. *Molecular Modelling: Principles and Applications*, 2nd ed.; Prentice Hall: Harlow, England ; New York, 2001.
(28) Klauda, J. B.; Venable, R. M.; Freites, J. A.; O'Connor, J. W.; Tobias, D. J.; Mondragon-Ramirez, C.; Vorobyov, I.; MacKerell, A. D. Jr.; Pastor, R. W. Update of the CHARMM All-Atom Additive Force Field for Lipids: Validation on Six Lipid Types. *J. Phys. Chem. B* **2010**, *114* (23), 7830–7843. https://doi.org/10.1021/jp101759q.
(29) Liu, Y.; Guan, P.; Wang, Y.; Liu, L.; Cao, J. Mechanistic Insight into Decomposition of 2H-Azirines: Electronic Structure Calculations and Dynamics Simulations. *J. Phys. Chem. A* **2015**, *119* (1), 67–78. https://doi.org/10.1021/jp511208p.
(30) Cao, J. Photoinduced Reactions of Both 2-Formyl-2H-Azirine and Isoxazole: A Theoretical Study Based on Electronic Structure Calculations and Nonadiabatic Dynamics Simulations. *The Journal of Chemical Physics* **2015**, *142* (24), 244302. https://doi.org/10.1063/1.4922742.
(31) Dickerson, C. E.; Bera, P. P.; Lee, T. J. Characterization of Azirine and Its Structural Isomers. *J. Phys. Chem. A* **2018**, *122* (45), 8898–8904. https://doi.org/10.1021/acs.jpca.8b07788.
(32) Cho, H.-G. Matrix Infrared Spectra and DFT Computations of 2H-Azirine Produced from Acetonitrile by Laser-Ablation Plume Radiation. *Bulletin of the Korean Chemical Society* **2014**, *35* (7), 2093–2096. https://doi.org/10.5012/bkcs.2014.35.7.2093.
(33) Zhu, B.; Zeng, X. 3-Fluoro-2H-Azirine: Generation, Characterization, and Photochemistry. *J. Phys. Chem. A* **2023**, *127* (50), 10591–10599. https://doi.org/10.1021/acs.jpca.3c06076.
(34) Wakchaure, P. D.; Ganguly, B. Tuning the Electronic Effects in Designing Ligands for the Inhibition of Rotamase Activity of FK506 Binding Protein. *Theor Chem Acc* **2021**, *140* (1), 5. https://doi.org/10.1007/s00214-020-02717-6.
(35) Duarte, V. C. M.; Faustino, H.; Alves, M. J.; Gil Fortes, A.; Micaelo, N. Asymmetric Diels–Alder Cycloadditions of d-Erythrose 1,3-Butadienes to Achiral t-Butyl 2H-Azirine 3-Carboxylate. *Tetrahedron: Asymmetry* **2013**, *24* (18), 1063–1068. https://doi.org/10.1016/j.tetasy.2013.05.015.
(36) Serratos, I. N.; Olayo, R.; Millán-Pacheco, C.; Morales-Corona, J.; Vicente-Escobar, J. O.; Soto-Estrada, A. M.; Córdoba-Herrera, J. G.; Uribe, O.; Gómez-Quintero, T.; Arroyo-Ornelas, M. Á.; Godínez-Fernández, R. Modeling Integrin and Plasma-Polymerized Pyrrole Interactions: Chemical Diversity Relevance for Cell Regeneration. *Sci Rep* **2019**, *9* (1), 7009. https://doi.org/10.1038/s41598-019-43286-4.
(37) Vanommeslaeghe, K.; MacKerell, A. D. Jr. Automation of the CHARMM General Force Field (CGenFF) I: Bond Perception and Atom Typing. *J. Chem. Inf. Model.* **2012**, *52* (12), 3144–3154. https://doi.org/10.1021/ci300363c.
(38) Dodda, L. S.; Cabeza de Vaca, I.; Tirado-Rives, J.; Jorgensen, W. L. LigParGen Web Server: An Automatic OPLS-AA Parameter Generator for Organic Ligands. *Nucleic Acids Research* **2017**, *45* (W1), W331–W336. https://doi.org/10.1093/nar/gkx312.
(39) Zwier, M. C.; Chong, L. T. Reaching Biological Timescales with All-Atom Molecular Dynamics Simulations. *Current Opinion in Pharmacology* **2010**, *10* (6), 745–752. https://doi.org/10.1016/j.coph.2010.09.008.
(40) Spiwok, V.; Sucur, Z.; Hosek, P. Enhanced Sampling Techniques in Biomolecular Simulations. *Biotechnology Advances* **2015**, *33* (6, Part 2), 1130–1140. https://doi.org/10.1016/j.biotechadv.2014.11.011.
(41) Allison, J. R. Computational Methods for Exploring Protein Conformations. *Biochemical Society Transactions* **2020**, *48* (4), 1707–1724. https://doi.org/10.1042/BST20200193.
(42) Doudou, S.; Burton, N. A.; Henchman, R. H. Standard Free Energy of Binding from a One-Dimensional Potential of Mean Force. *J. Chem. Theory Comput.* **2009**, *5* (4), 909–918. https://doi.org/10.1021/ct8002354.

(43) Trzesniak, D.; Kunz, A.-P. E.; van Gunsteren, W. F. A Comparison of Methods to Compute the Potential of Mean Force. *ChemPhysChem* **2007**, *8* (1), 162–169. https://doi.org/10.1002/cphc.200600527.
(44) Markthaler, D.; Jakobtorweihen, S.; Hansen, N. Lessons Learned from the Calculation of One-Dimensional Potentials of Mean Force [Article v1.0]. *Living Journal of Computational Molecular Science* **2019**, *1* (2), 11073–11073. https://doi.org/10.33011/livecoms.1.2.11073.
(45) Bussi, G.; Laio, A. Using Metadynamics to Explore Complex Free-Energy Landscapes. *Nat Rev Phys* **2020**, *2* (4), 200–212. https://doi.org/10.1038/s42254-020-0153-0.
(46) Barducci, A.; Bussi, G.; Parrinello, M. Well-Tempered Metadynamics: A Smoothly Converging and Tunable Free-Energy Method. *Phys. Rev. Lett.* **2008**, *100* (2), 020603. https://doi.org/10.1103/PhysRevLett.100.020603.
(47) Venable, R. M.; Sodt, A. J.; Rogaski, B.; Rui, H.; Hatcher, E.; MacKerell, A. D.; Pastor, R. W.; Klauda, J. B. CHARMM All-Atom Additive Force Field for Sphingomyelin: Elucidation of Hydrogen Bonding and of Positive Curvature. *Biophysical Journal* **2014**, *107* (1), 134–145. https://doi.org/10.1016/j.bpj.2014.05.034.
(48) Jorgensen, W. L.; Chandrasekhar, J.; Madura, J. D.; Impey, R. W.; Klein, M. L. Comparison of Simple Potential Functions for Simulating Liquid Water. *The Journal of Chemical Physics* **1983**, *79* (2), 926–935. https://doi.org/10.1063/1.445869.
(49) Beglov, D.; Roux, B. Finite Representation of an Infinite Bulk System: Solvent Boundary Potential for Computer Simulations. *The Journal of Chemical Physics* **1994**, *100* (12), 9050–9063. https://doi.org/10.1063/1.466711.
(50) Vanommeslaeghe, K.; Hatcher, E.; Acharya, C.; Kundu, S.; Zhong, S.; Shim, J.; Darian, E.; Guvench, O.; Lopes, P.; Vorobyov, I.; Mackerell Jr., A. D. CHARMM General Force Field: A Force Field for Drug-like Molecules Compatible with the CHARMM All-Atom Additive Biological Force Fields. *Journal of Computational Chemistry* **2010**, *31* (4), 671–690. https://doi.org/10.1002/jcc.21367.
(51) Kumar, A.; Yoluk, O.; MacKerell Jr., A. D. FFParam: Standalone Package for CHARMM Additive and Drude Polarizable Force Field Parametrization of Small Molecules. *Journal of Computational Chemistry* **2020**, *41* (9), 958–970. https://doi.org/10.1002/jcc.26138.
(52) Breneman, C. M.; Wiberg, K. B. Determining Atom-Centered Monopoles from Molecular Electrostatic Potentials. The Need for High Sampling Density in Formamide Conformational Analysis. *Journal of Computational Chemistry* **1990**, *11* (3), 361–373. https://doi.org/10.1002/jcc.540110311.
(53) Epifanovsky, E.; Gilbert, A. T. B.; Feng, X.; Lee, J.; Mao, Y.; Mardirossian, N.; Pokhilko, P.; White, A. F.; Coons, M. P.; Dempwolff, A. L.; Gan, Z.; Hait, D.; Horn, P. R.; Jacobson, L. D.; Kaliman, I.; Kussmann, J.; Lange, A. W.; Lao, K. U.; Levine, D. S.; Liu, J.; McKenzie, S. C.; Morrison, A. F.; Nanda, K. D.; Plasser, F.; Rehn, D. R.; Vidal, M. L.; You, Z.-Q.; Zhu, Y.; Alam, B.; Albrecht, B. J.; Aldossary, A.; Alguire, E.; Andersen, J. H.; Athavale, V.; Barton, D.; Begam, K.; Behn, A.; Bellonzi, N.; Bernard, Y. A.; Berquist, E. J.; Burton, H. G. A.; Carreras, A.; Carter-Fenk, K.; Chakraborty, R.; Chien, A. D.; Closser, K. D.; Cofer-Shabica, V.; Dasgupta, S.; de Wergifosse, M.; Deng, J.; Diedenhofen, M.; Do, H.; Ehlert, S.; Fang, P.-T.; Fatehi, S.; Feng, Q.; Friedhoff, T.; Gayvert, J.; Ge, Q.; Gidofalvi, G.; Goldey, M.; Gomes, J.; González-Espinoza, C. E.; Gulania, S.; Gunina, A. O.; Hanson-Heine, M. W. D.; Harbach, P. H. P.; Hauser, A.; Herbst, M. F.; Hernández Vera, M.; Hodecker, M.; Holden, Z. C.; Houck, S.; Huang, X.; Hui, K.; Huynh, B. C.; Ivanov, M.; Jász, Á.; Ji, H.; Jiang, H.; Kaduk, B.; Kähler, S.; Khistyaev, K.; Kim, J.; Kis, G.; Klunzinger, P.; Koczor-Benda, Z.; Koh, J. H.; Kosenkov, D.; Koulias, L.; Kowalczyk, T.; Krauter, C. M.; Kue, K.; Kunitsa, A.; Kus, T.; Ladjánszki, I.; Landau, A.; Lawler, K. V.; Lefrancois, D.; Lehtola, S.; Li, R. R.; Li, Y.-P.; Liang, J.; Liebenthal, M.; Lin, H.-H.; Lin, Y.-S.; Liu, F.; Liu, K.-Y.; Loipersberger, M.; Luenser, A.; Manjanath, A.; Manohar, P.; Mansoor, E.; Manzer, S. F.; Mao, S.-P.; Marenich, A. V.; Markovich, T.; Mason, S.; Maurer, S. A.; McLaughlin, P.

F.; Menger, M. F. S. J.; Mewes, J.-M.; Mewes, S. A.; Morgante, P.; Mullinax, J. W.; Oosterbaan, K. J.; Paran, G.; Paul, A. C.; Paul, S. K.; Pavošević, F.; Pei, Z.; Prager, S.; Proynov, E. I.; Rák, Á.; Ramos-Cordoba, E.; Rana, B.; Rask, A. E.; Rettig, A.; Richard, R. M.; Rob, F.; Rossomme, E.; Scheele, T.; Scheurer, M.; Schneider, M.; Sergueev, N.; Sharada, S. M.; Skomorowski, W.; Small, D. W.; Stein, C. J.; Su, Y.-C.; Sundstrom, E. J.; Tao, Z.; Thirman, J.; Tornai, G. J.; Tsuchimochi, T.; Tubman, N. M.; Veccham, S. P.; Vydrov, O.; Wenzel, J.; Witte, J.; Yamada, A.; Yao, K.; Yeganeh, S.; Yost, S. R.; Zech, A.; Zhang, I. Y.; Zhang, X.; Zhang, Y.; Zuev, D.; Aspuru-Guzik, A.; Bell, A. T.; Besley, N. A.; Bravaya, K. B.; Brooks, B. R.; Casanova, D.; Chai, J.-D.; Coriani, S.; Cramer, C. J.; Cserey, G.; DePrince, A. E., III; DiStasio, R. A., Jr.; Dreuw, A.; Dunietz, B. D.; Furlani, T. R.; Goddard, W. A., III; Hammes-Schiffer, S.; Head-Gordon, T.; Hehre, W. J.; Hsu, C.-P.; Jagau, T.-C.; Jung, Y.; Klamt, A.; Kong, J.; Lambrecht, D. S.; Liang, W.; Mayhall, N. J.; McCurdy, C. W.; Neaton, J. B.; Ochsenfeld, C.; Parkhill, J. A.; Peverati, R.; Rassolov, V. A.; Shao, Y.; Slipchenko, L. V.; Stauch, T.; Steele, R. P.; Subotnik, J. E.; Thom, A. J. W.; Tkatchenko, A.; Truhlar, D. G.; Van Voorhis, T.; Wesolowski, T. A.; Whaley, K. B.; Woodcock, H. L., III; Zimmerman, P. M.; Faraji, S.; Gill, P. M. W.; Head-Gordon, M.; Herbert, J. M.; Krylov, A. I. Software for the Frontiers of Quantum Chemistry: An Overview of Developments in the Q-Chem 5 Package. *The Journal of Chemical Physics* **2021**, *155* (8), 084801. https://doi.org/10.1063/5.0055522.

(54) Turney, J. M.; Simmonett, A. C.; Parrish, R. M.; Hohenstein, E. G.; Evangelista, F. A.; Fermann, J. T.; Mintz, B. J.; Burns, L. A.; Wilke, J. J.; Abrams, M. L.; Russ, N. J.; Leininger, M. L.; Janssen, C. L.; Seidl, E. T.; Allen, W. D.; Schaefer, H. F.; King, R. A.; Valeev, E. F.; Sherrill, C. D.; Crawford, T. D. Psi4: An Open-Source Ab Initio Electronic Structure Program. *WIREs Computational Molecular Science* **2012**, *2* (4), 556–565. https://doi.org/10.1002/wcms.93.

(55) Møller, Chr.; Plesset, M. S. Note on an Approximation Treatment for Many-Electron Systems. *Phys. Rev.* **1934**, *46* (7), 618–622. https://doi.org/10.1103/PhysRev.46.618.

(56) Binkley, J. S.; Pople, J. A.; Hehre, W. J. Self-Consistent Molecular Orbital Methods. 21. Small Split-Valence Basis Sets for First-Row Elements. *J. Am. Chem. Soc.* **1980**, *102* (3), 939–947. https://doi.org/10.1021/ja00523a008.

(57) Xu, F.; Zeng, F.-W.; Luo, W.-J.; Zhang, S.-Y.; Huo, J.-Q.; Li, Y.-P. 2H-Azirines: Recent Progress in Synthesis and Applications. *Eur J Org Chem* **2024**, e202301292. https://doi.org/10.1002/ejoc.202301292.

(58) Carreiras, M. do C.; Marco-Contelles, J. *Heterocyclic Targets in Advanced Organic Synthesis*; Research Signpost: Kerala, India, 2011.

(59) Jo, S.; Lim, J. B.; Klauda, J. B.; Im, W. CHARMM-GUI Membrane Builder for Mixed Bilayers and Its Application to Yeast Membranes. *Biophysical Journal* **2009**, *97* (1), 50–58. https://doi.org/10.1016/j.bpj.2009.04.013.

(60) Jo, S.; Kim, T.; Im, W. Automated Builder and Database of Protein/Membrane Complexes for Molecular Dynamics Simulations. *PLOS ONE* **2007**, *2* (9), e880. https://doi.org/10.1371/journal.pone.0000880.

(61) Lee, J.; Patel, D. S.; Ståhle, J.; Park, S.-J.; Kern, N. R.; Kim, S.; Lee, J.; Cheng, X.; Valvano, M. A.; Holst, O.; Knirel, Y. A.; Qi, Y.; Jo, S.; Klauda, J. B.; Widmalm, G.; Im, W. CHARMM-GUI Membrane Builder for Complex Biological Membrane Simulations with Glycolipids and Lipoglycans. *J. Chem. Theory Comput.* **2019**, *15* (1), 775–786. https://doi.org/10.1021/acs.jctc.8b01066.

(62) Wu, E. L.; Cheng, X.; Jo, S.; Rui, H.; Song, K. C.; Dávila-Contreras, E. M.; Qi, Y.; Lee, J.; Monje-Galvan, V.; Venable, R. M.; Klauda, J. B.; Im, W. CHARMM-GUI Membrane Builder toward Realistic Biological Membrane Simulations. *Journal of Computational Chemistry* **2014**, *35* (27), 1997–2004. https://doi.org/10.1002/jcc.23702.

(63) Murzyn, K.; Róg, T.; Pasenkiewicz-Gierula, M. Phosphatidylethanolamine-Phosphatidylglycerol Bilayer as a Model of the Inner Bacterial Membrane. *Biophysical Journal* **2005**, *88* (2), 1091–1103. https://doi.org/10.1529/biophysj.104.048835.
(64) Hanwell, M. D.; Curtis, D. E.; Lonie, D. C.; Vandermeersch, T.; Zurek, E.; Hutchison, G. R. Avogadro: An Advanced Semantic Chemical Editor, Visualization, and Analysis Platform. *J Cheminform* **2012**, *4* (1), 17. https://doi.org/10.1186/1758-2946-4-17.
(65) Eastman, P.; Swails, J.; Chodera, J. D.; McGibbon, R. T.; Zhao, Y.; Beauchamp, K. A.; Wang, L.-P.; Simmonett, A. C.; Harrigan, M. P.; Stern, C. D.; Wiewiora, R. P.; Brooks, B. R.; Pande, V. S. OpenMM 7: Rapid Development of High Performance Algorithms for Molecular Dynamics. *PLOS Computational Biology* **2017**, *13* (7), e1005659. https://doi.org/10.1371/journal.pcbi.1005659.
(66) Park, S.; Choi, Y. K.; Kim, S.; Lee, J.; Im, W. CHARMM-GUI Membrane Builder for Lipid Nanoparticles with Ionizable Cationic Lipids and PEGylated Lipids. *J. Chem. Inf. Model.* **2021**, *61* (10), 5192–5202. https://doi.org/10.1021/acs.jcim.1c00770.
(67) Smith, D. J.; Klauda, J. B.; Sodt, A. J. Simulation Best Practices for Lipid Membranes [Article v1.0]. *Living Journal of Computational Molecular Science* **2019**, *1* (1), 5966–5966. https://doi.org/10.33011/livecoms.1.1.5966.
(68) Chow, K.-H.; Ferguson, D. M. Isothermal-Isobaric Molecular Dynamics Simulations with Monte Carlo Volume Sampling. *Computer Physics Communications* **1995**, *91* (1), 283–289. https://doi.org/10.1016/0010-4655(95)00059-O.
(69) Izaguirre, J. A.; Sweet, C. R.; Pande, V. S. Multiscale Dynamics of Macromolecules Using Normal Mode Langevin. In *Biocomputing 2010*; WORLD SCIENTIFIC, 2009; pp 240–251. https://doi.org/10.1142/9789814295291_0026.
(70) Ermilova, I.; Lyubartsev, A. P. Cholesterol in Phospholipid Bilayers: Positions and Orientations inside Membranes with Different Unsaturation Degrees. *Soft Matter* **2019**, *15* (1), 78–93. https://doi.org/10.1039/C8SM01937A.
(71) Jämbeck, J. P. M.; Lyubartsev, A. P. Exploring the Free Energy Landscape of Solutes Embedded in Lipid Bilayers. *J. Phys. Chem. Lett.* **2013**, *4* (11), 1781–1787. https://doi.org/10.1021/jz4007993.
(72) Bochicchio, D.; Panizon, E.; Ferrando, R.; Monticelli, L.; Rossi, G. Calculating the Free Energy of Transfer of Small Solutes into a Model Lipid Membrane: Comparison between Metadynamics and Umbrella Sampling. *The Journal of Chemical Physics* **2015**, *143* (14), 144108. https://doi.org/10.1063/1.4932159.
(73) Branduardi, D.; Bussi, G.; Parrinello, M. Metadynamics with Adaptive Gaussians. *J. Chem. Theory Comput.* **2012**, *8* (7), 2247–2254. https://doi.org/10.1021/ct3002464.
(74) Schäfer, T. M.; Settanni, G. Data Reweighting in Metadynamics Simulations. *J. Chem. Theory Comput.* **2020**, *16* (4), 2042–2052. https://doi.org/10.1021/acs.jctc.9b00867.
(75) Helmkamp, G. M. Effects of Phospholipid Fatty Acid Composition and Membrane Fluidity on the Activity of Bovine Brain Phospholipid Exchange Protein. *Biochemistry* **1980**, *19* (10), 2050–2056. https://doi.org/10.1021/bi00551a007.
(76) Niu, S.-L.; Mitchell, D. C.; Litman, B. J. Trans Fatty Acid Derived Phospholipids Show Increased Membrane Cholesterol and Reduced Receptor Activation as Compared to Their Cis Analogs. *Biochemistry* **2005**, *44* (11), 4458–4465. https://doi.org/10.1021/bi048319+.
(77) Alberts, B.; Johnson, A.; Lewis, J.; Raff, M.; Roberts, K.; Walter, P. The Lipid Bilayer. In *Molecular Biology of the Cell. 4th edition*; Garland Science, 2002.
(78) Entova, S.; Guan, Z.; Imperiali, B. Investigation of the Conserved Reentrant Membrane Helix in the Monotopic Phosphoglycosyl Transferase Superfamily Supports Key Molecular Interactions with Polyprenol Phosphate Substrates. *Archives of Biochemistry and Biophysics* **2019**, *675*, 108111. https://doi.org/10.1016/j.abb.2019.108111.

(79) Ernst, A. M.; Contreras, F. X.; Brügger, B.; Wieland, F. Determinants of Specificity at the Protein–Lipid Interface in Membranes. *FEBS Letters* **2010**, *584* (9), 1713–1720. https://doi.org/10.1016/j.febslet.2009.12.060.
(80) Choo, M. Z. Y.; Chai, C. L. L. The Polypharmacology of Natural Products in Drug Discovery and Development. In *Annual Reports in Medicinal Chemistry*; Elsevier, 2023; Vol. 61, pp 55–100. https://doi.org/10.1016/bs.armc.2023.10.002.
(81) Nicolson, G. L.; Ferreira de Mattos, G. A Brief Introduction to Some Aspects of the Fluid–Mosaic Model of Cell Membrane Structure and Its Importance in Membrane Lipid Replacement. *Membranes* **2021**, *11* (12), 947. https://doi.org/10.3390/membranes11120947.

# TOC Image